Evaluating Severity of Impact Damage in CFRP by Determining Thermal Effusivity and Diffusivity

V.P. VAVILOV, A.O. CHULKOV, D.A. DERUSOVA
Institute of Nondestructive Testing
Tomsk Polytechnic University
30 Lenin Av, Tomsk, 634050
RUSSIA
vavilov@tpu.ru   http://www.tpu.ru

Abstract: - The goal of this study is the analysis of some candidate defect characterization parameters in application to the detection of impact damage in carbon fiber reinforced polymers. It is shown that quantitative evaluation of 'defectivity' aimed to further estimation of material strength, or lifetime, should be done by determining material thermal properties. Experimental results obtained are related to active thermal nondestructive testing of aviation panels with impact damage. The efficiency of some image processing algorithms, such as principal component analysis, Fourier and wavelet transform, has been evaluated. It has been found that the result of image sequence processing should be an image of diffusivity in a two-sided procedure and image of effusivity in a one-sided procedure.

Key-Words: - thermal nondestructive testing, heat conduction, effusivity, diffusivity, image processing

1 Introduction

Fundamentals of active thermal nondestructive testing (NDT) are well-known [1-3]. Theoretically, this technique is based on solutions to direct heat conduction problems thus predicting temperature signals and their observation times as functions of heating parameters and material/defect thermal properties. Theoretical predictions are normally in a good accordance with experimental data, hence, the proposed 2D and 3D numerical models are trust-worthy. In parallel, there is a growing interest to the solutions of inverse thermal NDT problems intended for the estimation of defect parameters ('defect characterization' procedures) [4]. In mathematics, inverse solutions are considered to be incorrect, i.e. having no accurate solutions, but, in practice, numerous robust formulas have been proposed to evaluate defect depth and size.

Recently, one more aspect in the theory of thermal NDT appeared being related to the quantitative evaluation of defect severity [5]. This aspect is important for the evaluation of material long-lasting strength (component lifetime). In fact, one needs to find a parameter of temperature distributions which will uniquely characterize defect severity. The need for the corresponding research comes, for example, from the aero space industry where impetuous growth of the use of composites has put new challenges for NDT. In fact, it is

believed that all airplanes under exploitation contain of minor defects, such as impact damage in panels made of carbon fiber reinforced polymer (CFRP), and, because of the aggressive effect of the atmosphere, these minor defects may transit into serious ones.

In this study, we analyze some candidate characterization parameters in application to the detection of impact damage in CFRP.

2 Thermal NDT Models

According to the scheme of thermal NDT by applying external thermal stimulation (Fig. 1), a regular heat flux generated by a heat source is disturbed by subsurface defects thus causing appeared abnormal temperature signals on both the front and rear surfaces. These signals are recorded by an IR imager as a sequence of infrared (IR) thermograms which are characterized by $T(i, j)$ pixel functions.

Very often such inspection procedure is limited by defect detection only that is done either by a trained operator or an automatic device. A more complicated is the defect characterization procedure which requires the use of some sophisticated processing algorithms and is supposed to result in estimates of defect depth l, thickness d and lateral dimensions h_y, h_y (Fig. 1). Such algorithms are

developed by solving the corresponding problems of heat conduction in solids with hidden structural irregularities (defects).
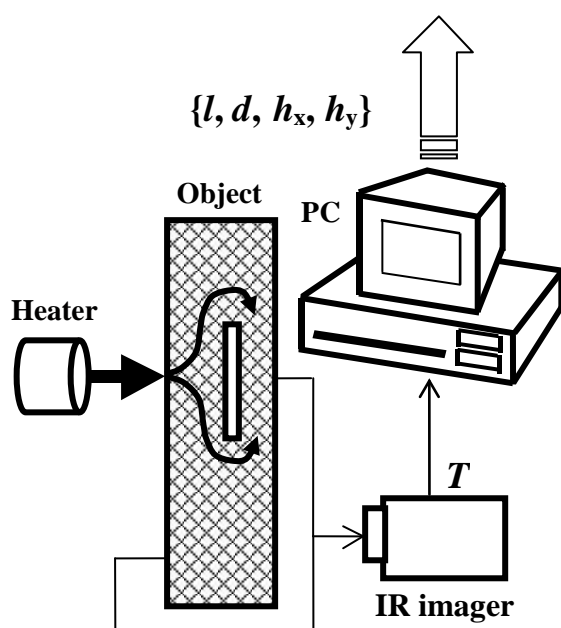

Fig.1. Active thermal NDT scheme.

Below we will generalize some theoretical models widely used in thermal NDT theoretical models. Consider the detection of impact damage in a composite material as a typical defect occurring in aviation panels during aircraft exploitation. On the front (F) surface, there is typically a minor, if any, visible damage, while a major body of the defect consisting of vast multiple cracks appear closer to the rear (R) surface (Fig. 2, model M1). The real defect situation can be modeled either in the cylindrical 2D or in the Cartesian 3D geometry with multiple (M2) or single (M3) defects. Multiple defects (M2) may represent some parallelepipeds (or disks) of different size located at different depths. In the simplest case, they can be replaced with a single parallelepiped-like (or disk-like) defect (M3). Models in Fig. 2 are typically analyzed by using numerical methods. Analytical solutions can be obtained in 1D geometries where defect lateral dimensions are much greater than their depth (by 6-10 times depending on a material). In this case, defect and non-defect areas are analyzed independently, and the differential temperature signal is $\Delta T(\tau) = T_d(\tau) - T_{nd}(\tau)$. The most convenient 1D model involves a three-layer plate where a central layer represents either a host material or a defect (Fig. 2, model M4). Finally, the presence of a defect can be regarded as a local

material loss (the so-called bottom-hole defects [6]) with no heat conduction through the defect (M5). In the latter case, on the rear surface, $\Delta T(\tau) = T_d(\tau)$.

Evolutions of temperature in time for all models above are presented in Fig. 3. Thermal properties are assumed for an anisotropic CFRP as follows: thermal conductivities by three coordinates K_x=8.74 W/(m·°C), K_y=0.611 W/(m·°C), K_z=0.619 W/(m·°C); thermal diffusivities a_x=44.6·10^{-7} m²/s, a_y=3.12·10^{-7} m²/s, a_z=3.16·10^{-7} m²/s, specific heat C=1411 J/(kg·°C), density ρ=1652 kg/m³. An air-filled defect is located at the depth of 2.45 mm in a 5 mm-thick sample. Defect thickness is 0.1 mm and its lateral area is 0.785 cm². In the cylindrical (2D) geometry this is a disk with the diameter of 1 cm, while in the Cartesian (3D) geometry the defect laterally represents a square with the size of 15.7x5 mm. The sample is uniformly heated with a 10 kW/m² heat flux for 10 seconds.

The close results which are supposed to reflect practical cases appear in both the 2D and 3D models (curves M3 in Fig. 3). A small discrepancy in ΔT values is due to a stretched shape of the defect in the 3D case and a higher conductivity in X direction K_x. Qualitatively, similar results are provided by the 1D case (3-layer sample, curve M4 in Fig. 3), at least, in regard to the so-called optimum observation time τ_m which correspond to the maximum ΔT_m value. However, there is a 6-fold difference in amplitude between 1D and 2D (3D) cases that is explained by lateral heat diffusion. Finally, the model of a laterally-infinite bottom-hole defect seems to be unacceptable by both ΔT_m and τ_m values (curve M5 in Fig. 3, notice that values are divided by 10). The above-mentioned features of the discussed models keep for both one- and two-sided procedures.

It is worth noting that the thermal NDT models discussed above are quite general, however, they cannot be applied to the so-called 'kissing' defects and the cases where material thermal properties vary in time and/or space. A special situation is represented by thermal NDT problems which involve phase transformations, such as evaporation and freezing. In such cases, more advanced models are to be developed [7-9].
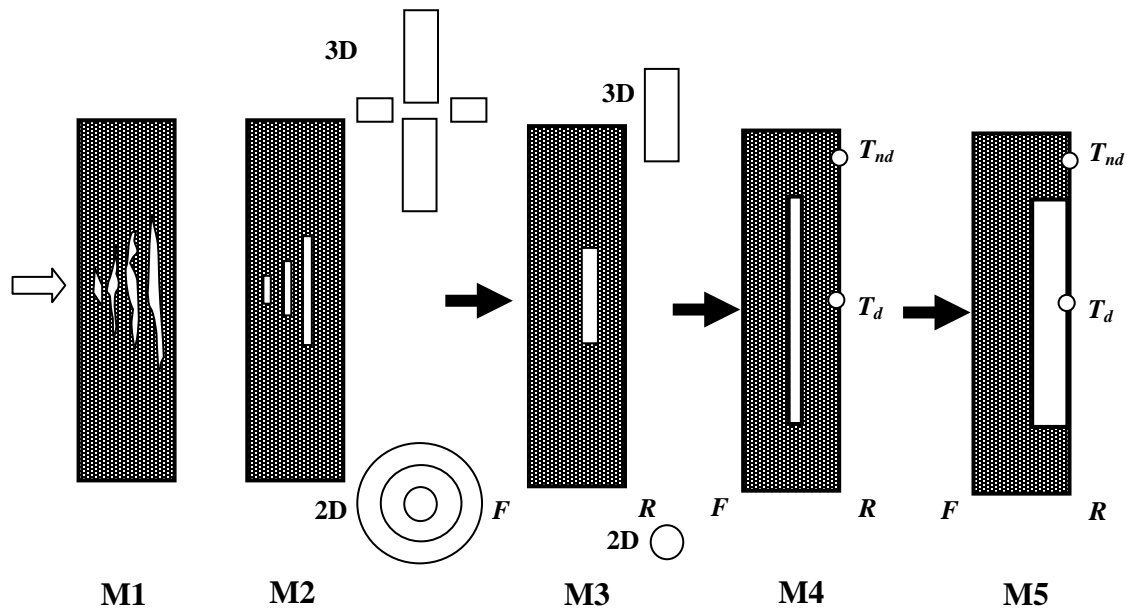
Fig. 2. Modeling impact damage in a composite material

.

3 Determining Thermal Properties: A Simple Theory

The determination of material thermal properties is a vast independent area of intensive research where thermal conductivity K, specific heat C, and density ρ are being determined in both stationary and dynamic procedures [10-12]. In application to thermal NDT, it is commonly assumed that a thermal parameter which adheres to a one-sided procedure is thermal effusivity e while thermal diffusivity a appears in two-sided heat conduction solutions.

In the evident form, effusivity can be derived from the known solution for heating an adiabatic semi-infinite body with a Dirac pulse. At any time τ:

$$T^F(\tau) = \frac{W}{e\sqrt{\pi\tau}} \; ; \tag{1}$$

$$e = \frac{W}{T^F(\tau)\sqrt{\pi\tau}} \tag{2}$$

where T is the temperature, and W is the absorbed energy, $e = \sqrt{KC\rho}$ is the thermal effusivity. Obviously, even in the case of a semi-infinite body, that is not typical in practice, it is impossible to determine the C, K and ρ separately but only as

a complex $e = \sqrt{C\rho K}$. Besides, it is indispensable to know absorbed energy in each surface point that practically difficult. For instance, in the ThermoFit Pro software (Tomsk Polytechnic University, Russia), the following pixel-based parameter can be determined:

$$\frac{e}{W} = \frac{1}{T^F(\tau)\sqrt{\pi\tau}} \; . \tag{3}$$

Since $e \sim 1/T^F$, from the point of view of the quantitative analysis in thermal NDT, the effusivity parameter gives no advantage compared to temperature. Moreover, dividing by noisy temperature function may only increase the overall noise.

Another important formula often used in the thermal NDT theory is the solution for the heating of an adiabatic plate with a Dirac pulse:

$$T^F = (Wa/KL)\,\theta_D^F \; ;$$

$$\theta_D^F = 1 + 2\sum_{n=1}^{\infty} e^{-n^2\pi^2 Fo} , \tag{4}$$

where $Fo = a\tau/L^2$ is the Fourier number, and L is the plate thickness.

a)

b)
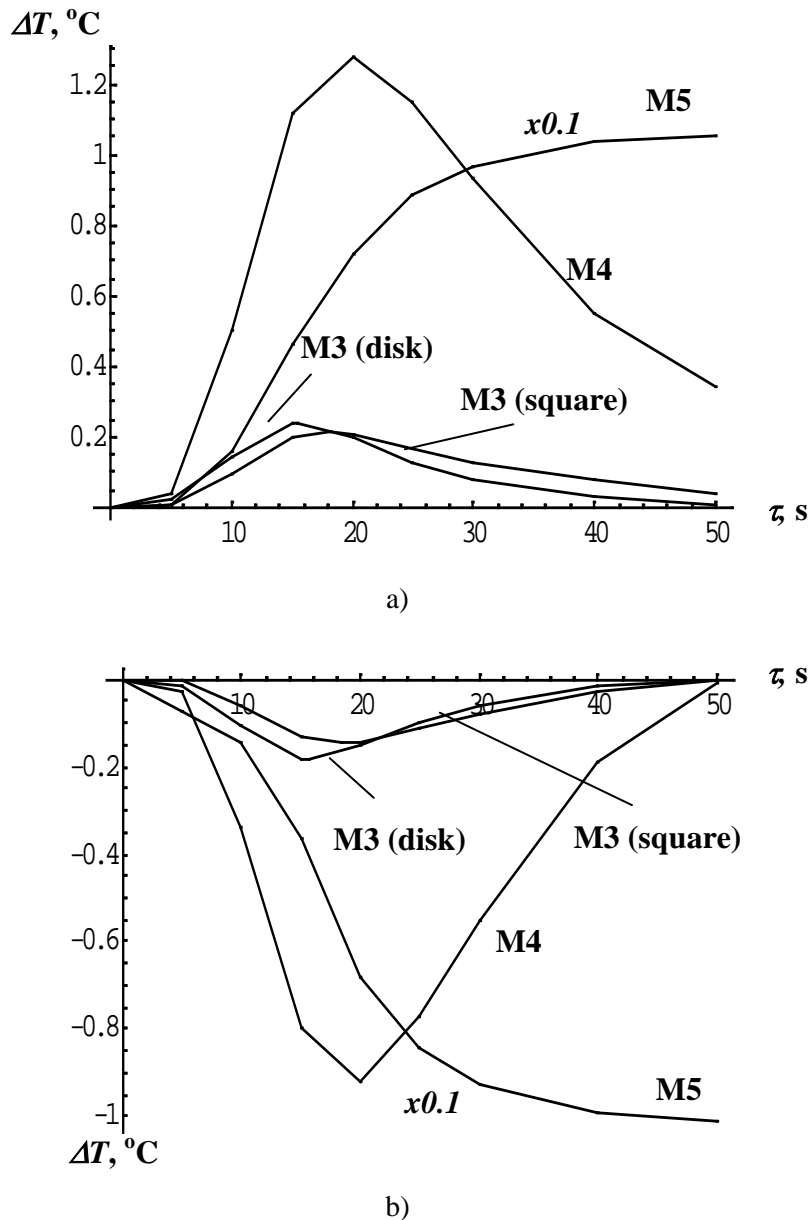
Fig. 3. Differential temperature signals over defects in the models by Fig. 1:

a – one-sided test (front surface),
b – two-sided test (rear surface)

Eq. (1) can be written in the form:

$$\frac{T^F(\tau)}{Wa/KL} = \frac{1}{\sqrt{\pi Fo}} . \qquad (5)$$

Then, the curves 1 and 2 describing the functions by Eq. (4) and Eq. (5) will be as shown in Fig. 4. Until $Fo \sim 0.2$, both solutions produce identical values of temperature and, at later times, the front surface temperature starts to 'sense' the rear surface of a plate. At $Fo \rightarrow \infty$ the plate temperature acquires its stationary value Wa/KL, while the temperature of a semi-infinite body drops down to

zero (note that in both cases $T \rightarrow \infty$ if $\tau \rightarrow 0$. However, in practice, the plate temperature also decreases up to the initial one due to heat exchange with the ambient, therefore, it is difficult to find some characteristic points in a front-surface response in order to determine a.

Thermal diffusivity, in its classical form, is adhered to the two-sided solution for heating a plate of the thickness L with a Dirac pulse:

$$T^R = (Wa/KL)\,\theta_D^R;$$

$$\theta_D^R = 1 + 2\sum_{n=1}^{\infty}(-1)^n\,e^{-n^2\pi^2 Fo}, \qquad (6)$$

where the superscript «R» specifies a rear surface.
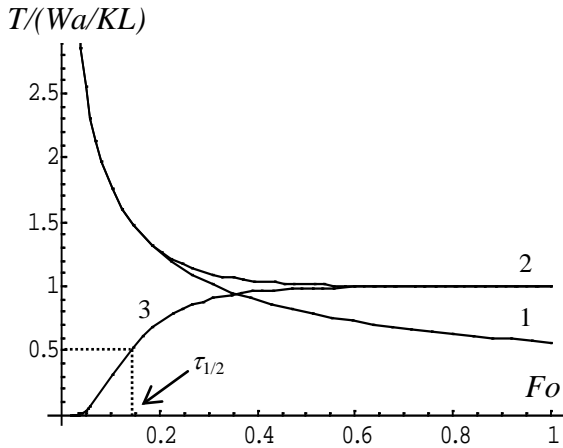
Fig. 4. Adiabatic heating with a Dirac heat pulse (1 - semi-infinite body, 2 - plate, front surface, 3-plate, rear surface)

The corresponding curve 1 is shown in Fig. 4. Since this curve starts from zero and reaches an evident maximum, particularly, in a non-adiabatic case, one may find some specific time $\tau*$ points for determining a, as suggested by Parker et al. [10]:

$$a = Fo*\frac{L^2}{\tau*}, \qquad (7)$$

where, for example, $Fo* = 0.1388$, if the so-called half-rise time $\tau* = \tau_{1/2}$ is chosen on the rear-surface temperature response curve (see Fig. 4). Other relative temperature levels for the calculation of $\tau*$ can be chosen but all they require reaching the maximum value. Another solution is to choose a time point $\tau_{m.d.}$ when the first derivative of rear-surface response by time acquires its maximum value. In this case, there is no need to reach a

maximum value, and the diffusivity can be determined by the following formula: $a = 0.0918\,L^2/\tau_{m.d.}$. Since derivation tends to increase noise, this approach is typically applied to fitted functions.

The front-surface temperature T^F curve can be used for determining diffusivity in each surface point by applying non-linear fitting [12] but this procedure is time-consuming and its efficiency is lower than in the case of the corresponding two-sided procedure.

On a front surface, a specific heat transit time, similar to $\tau_{1/2}$, can be created artificially, for example, by introducing the following function:

$$T' = Fo^n\,T_D^F, \qquad (8)$$

which reaches minimum at a particular time. For example, $Fo*$=0.2656 if n=1/3 (see Fig. 5). However, the minimum of the curve in Fig. 5 looks quite flat; therefore, this approach is susceptible to noise. It is interesting to note that the transformation by Eq. (8), being applied to defect areas, leads to very different functions compared to Fig. 5. The use of this approach for the detection of subsurface defects needs further exploration.

4 Experimental results

In order to illustrate a choice of defect characterization parameters, a 4.7 mm-thick CFRP specimen was tested in both one- and two-sided thermal NDT procedures by applying square pulse heating with 2 kW halogen lamps and flash heating with 3.2 kJ Xenon tubes (one-sided approach only). The sample contained 10 J impact damage; the acquisition time interval was 0.1 s in the first and 0.017 s in the second case. IR image sequences were analyzed with the ThermoLab software (Tomsk Polytechnic University) by applying three algorithms: Fourier and wavelet transforms? and principle component analysis (PCA).
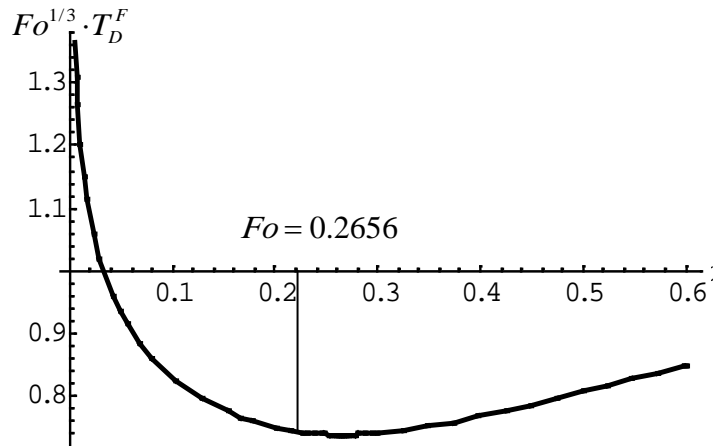
Fig. 5. Evolution of $Fo^{1/3} \cdot T_D^F$ function in time on the front surface of a plate heated with a Dirac pulse

The images of the sample (Fig. 6) have been visually evaluated with some comments being presented in Table 1. The goal of the evaluation has been to recommend an optimal evaluation parameter which can be used in the future for establishing connection between this parameter and defect severity. The results in Fig. 6 show that some popular data treatment algorithms, such as integral transforms and PCA, may provide a better defect detection but in many such cases a signal topology is not monotonous. For defect characterization, in a two-sided procedure, the most convenient are images of diffusivity which are obtained in the time domain thus being essentially free of the noise caused by absorptivity/emissivity variations.

In a one-sided procedure, a decision-making parameter is still to be chosen. In fact, one should replace the amplitude-domain data treatment with time-domain, similarly to the one-sided procedure. A possible approach can be that given in Fig. 5.

The ambiguous behavior of signals after having applied the above-mentioned processing algorithms makes difficult a decent comparison of data processing algorithms that is typically done by using signal-to-noise ratio S. Very often, to calculate S, it is suggested to define a defect (D) and non-defect (ND) areas on sample surface (Fig. 7), and afterwards to apply the following formula:

$$S = \frac{(\sum_{i=1}^{M} T_i - \bar{T}_{nd})/M}{\sigma_{nd}}, \qquad (9)$$

where T_i is the temperature (or any other signal) in the i-th pixel of a defect area, $\bar{T}_{nd}$ is the mean temperature in a sound area, σ_{nd} is the temperature standard deviation in a non-defect area., and M is the number of pixels in a chosen defect area. It is obvious that, if a defect area is characterized by signals of opposite signs in respect to the background, S values become lower even if visually defect areas are clearly seen. This phenomenon appears if a defect area consists of some sub-areas of which temporal behavior is different from that of the background.

Table1. Features of image processing algorithms

Image	Description
Source IR thermogram	Temperature is a monotonous function of defect parameters but strongly depends on heating parameters.
Fourier phasegram	Fourier phase is an ambiguous function of defect parameters and independent of heating power.
Wavelet phasegram	Features of this algorithm are not well explored but similar to Fourier.
PCA image	PCA images reflect various features of temperature evolution but in an ambiguous way.
Effusivity image	By the very concept, effusivity images should reflect differences in thermal properties but they are sensitive to heating power, sample thickness and heat pulse duration.
Diffusivity image	Diffusivity image represents a stable characteristic of a tested sample. It is fairly independent on heating power and might be used for defect identification.

a)   b)   c)   d)   e)

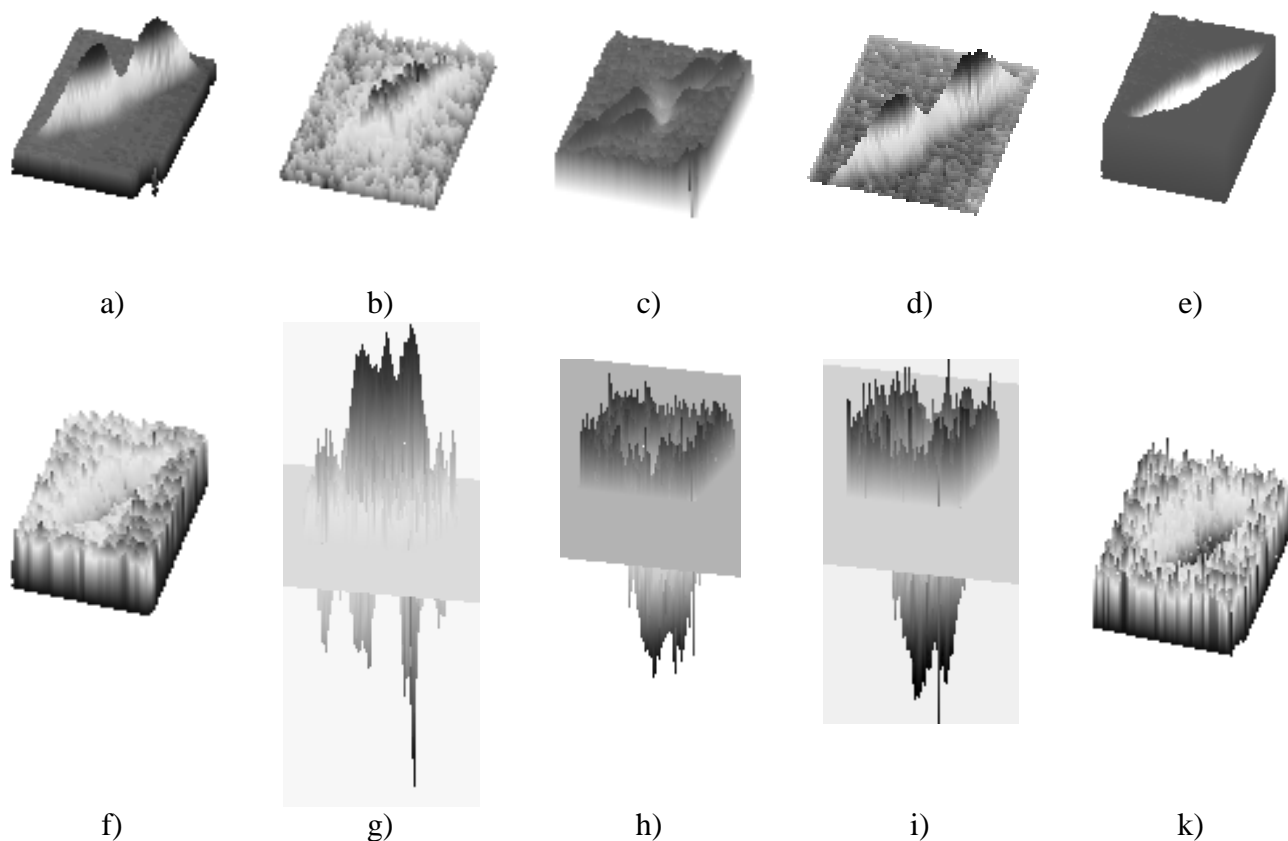f)   g)   h)   i)   k)

Fig. 6. Impact damage image processing (a-e: one-sided test, f-k: two-sided test):

a, f – source images,
b, g – Fourier phasegrams,
c, h – wavelet phasegrams,
d, i – PCA images,
e – effusivity image,
k – diffusivity image
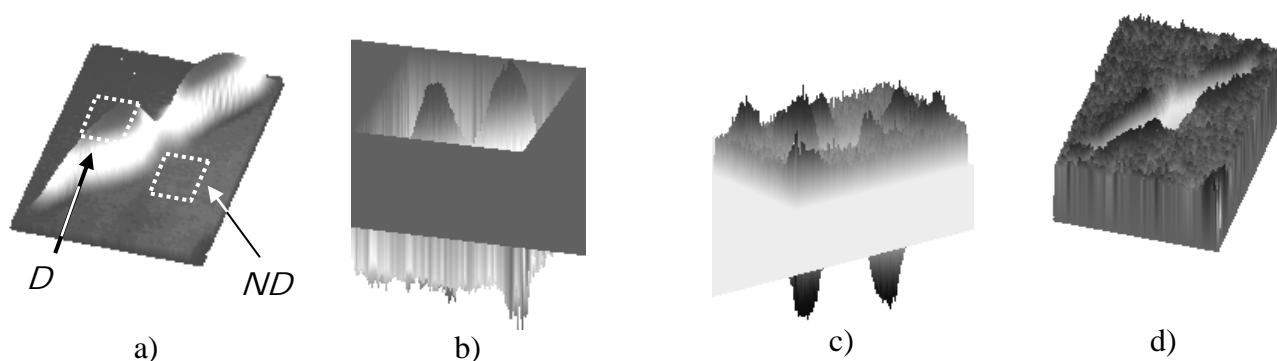

D   ND

a)   b)   c)   d)

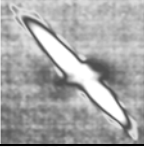Fig. 7. Calculating signal-to-noise ratio by Eq. (9) (flash heating of a 4.7 mm-thick CFRP sample):

a - best source image (S=127),
b - Fourier phasegram (S=184),
c - PCA image (S=161),
d - wavelet phasegram (S=196)

In this study, we suggest to use the modified expression for S:

$$S = \frac{(\sum_{i=1}^{M} |\bar{T}_i - \bar{T}_{nd}|)/M}{\sigma_{nd}}. \qquad (10)$$

The difference between two definitions of S by Eq. (9) and Eq. (10) is illustrated in Table 2. It is seen that the optimum processing algorithm, by using Eq. (10), is the wavelet analysis resulting in a wavelet phasegram, as shown in Fig. 7d (S=.196).

Table 2. Optimizing image processing algorithms

Algorithm	Image	S	
		by Eq.(9)	by Eq.(10)
Source IR thermogram		127	127
Fourier phasegram		13	184
Wavelet phasegram		17	196
PCA image		19	161

5 Diffusivity vs. impact energy

The final goal of this study was to analyze a relationship between impact energy W_{imp} and a relative variation of diffusivity $\Delta a / a$ in CFRP. Eight CFRP samples with the thickness from 1.7 to 5 mm which contained sites of impact damage of different energy were inspected by applying a two-sided procedure (classical Parker's technique of diffusivity measurement). The samples were impacted on the front surface where composite damage was hardly visible, and the temperature distribution was thermographically monitored on both surfaces. The results obtained with the ThermoLab software are given in Table 3. It is worth noting that IR thermograms might be very

different on front and rear surfaces but the determined variations of diffusivity appear to be identical. This is obvious since in fact the material diffusivity in defect and sound areas has been measured in all tests. The $\Delta a / a$ vs. W_{imp} relationship obtained by fitting the data in Table 3 with a second-order polynomial is shown in Fig. 7 along with experimental points. One point $\Delta a / a$ =2.2% has been excluded from the consideration as an extreme case, and the corresponding curve is described with the following function:

$$\Delta a / a = 9.33 - 0.166\, W_{imp} + 0.0119\, W_{imp}^2 \qquad (11)$$

Note that the function by Eq. (11) combines the data for 'thin' and 'thick' samples that can be incorrect due to differences in damage strength. Also, the considerable spread in $\Delta a / a$ might be explained not only by experimental errors but by the fact that the damage severity may vary even for identical samples depending on the composite structure in a hit point. Therefore, the results presented in Table 3 and Fig. 8 are regarded as preliminary thus requiring more statistics to be involved. However, these results are illustrative to hypothesize that the energy of impact damage in composites can be evaluated by determining variation in diffusivity.
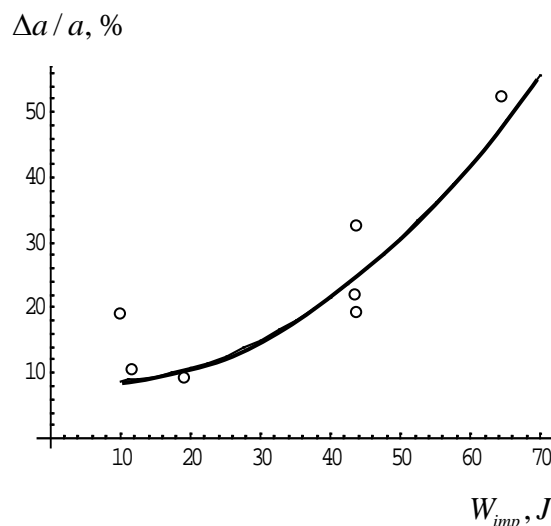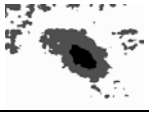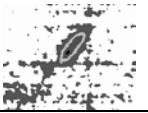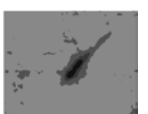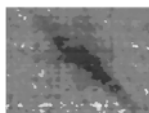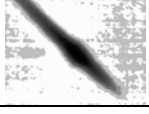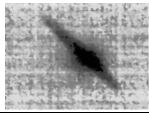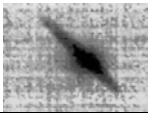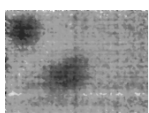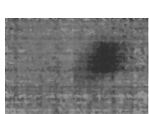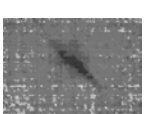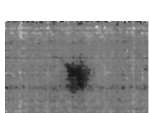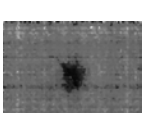

Fig. 8. Diffusivity variation vs. impact energy in CFRP samples

Table 3. Diffusivity variation vs. impact energy in CFRP samples

Sample thick-ness, mm	Impact energy, J	$\Delta a / a$, %	Front surface image	Rear surface image
1.7	10.0	20.0		
1.8	10.1	11.9		
1.7	10.0	2.2		
1.6	17.9	58.6		
4.7	62.4	49.7		
4.6	46.0	18.8		
4.8	45.5	17.9		
4.6	46.7	34.4		

6 Conclusion

Infrared thermographic NDT supplies versatile information about temperature behavior in time and space. Therefore, there are many available image processing techniques which are either general or heat conduction related. Very typical are Fourier and wavelet transforms, and PCA. These techniques have proven to be sensitive to subtle variations of temperature distributions thus significantly improving defect 'visibility', particularly if defect detection is accomplished

by an operator. The comparison of various processing algorithms by using a signal-to-noise ratio should be done carefully because some defect areas might look oppositely compared to the background. A conventional formula for calculating a signal-to-noise ratio should be modified by introducing absolute values of the differences between 'defective' pixels and a chosen sound area. By applying this approach to a particular case of the detection of impact damage in CFRP, it has been found that the highest signal-to-noise ratio appears while applying the wavelet transform. However, a quantitative evaluation of 'defectivity' aimed to further estimation of material strength, or lifetime, should be done by determining material thermal properties. In fact, the result of the processing of image sequences should be an image of diffusivity in a two-sided procedure and image of effusivity (or raw temperature image) in a one-sided procedure. A novel technique allowing the determination of diffusivity in a one-sided procedure by manipulating the front-surface temperature response is under development.

In the future, it is planned to analyze the relationship between the mechanical strength of damaged composites and changes in the proposed thermal NDT parameters, such as effusivity and diffusivity.

References:

[1] V. Vavilov, R. Taylor, Theoretical and Practical Aspects of the Thermal NDT of Bonded Structures, In: *Res. Techn. in NDT*, vol.5, ed. by R. Sharpe, Academic Press, London, U.K., 1982, pp.239-280.

[2] V.P. Vavilov, Pulsed Thermal NDT of Materials: Back to Basics, *Nondestr. Testing & Evaluation*, Taylor & Fransis, Great Britain, vol. 22, no.2-3, 2007, pp.177-198.

[3] X. Maldague, *Theory and Practice of Infrared Technology for Nondestructive Testing, Wiley Series in Microwave and Optical Engineering*, John Wiley & Sons, New York, U.S.A., 2001.

[4] D. Maillet, S. Andre, J.-C. Batsale, A. Degiovanni, C. Moyne, *Thermal Quadrupoles: Solving the Heat Equation Through Integral Transforms*, John Wiley & Sons Publ., England, 2000.

[5] M. Melis, J. Brand, J. Pereira, D. Revilock, Reinforced Carbon-Carbon Subcomponent Flat Plate Impact Testing for Space Shuttle Orbiter Return to Flight, *Proc. 2006 National Space and Missile Materials Symposium (NSMMS)*, Orlando, USA, June 26-30, 2006, pp. 1-23.

[6] D.J. Roth, J.R. Bodis, C. Bishop, Capability of Single-Sided Transient Thermographic Imaging Method for Detection of Flat Bottom Hole Defects in High-Temperature Composite Materials, *Rev. of Progress in Quant. Nondestr. Evaluation*, vol. 16, 1997, pp. 1127-1134.

[7] L. Garbai, S. Mehes, New Analytical Solutions to Determine the Temperature Field in Unsteady Heat Conduction, *WSEAS Transactions on Heat and Mass Transfer*, vol. 1, no. 7, July 2006, pp. 677-685.

[8] V.P. Vavilov, D. Burleigh, V.G. Demin, Advanced Modeling of Thermal NDT Problems: from Buried Landmines to Defects in Composites, *Proc. SPIE "Thermosense XXIV"*, vol. 4710, pp. 507-521.

[9] M. Buike, A. Buikis. Modelling of Three-Dimensional Transport Processes in Anisotropic Layered Stratum by Conservative Averaging Method, *WSEAS Transactions on Heat and Mass Transfer*, vol. 1, no. 4, April 2006, pp. 430-437.

[10] W.J. Parker, R.J. Jenkins, C.P. Butler, G.L. Abbot, Flash Method of Determining Thermal Diffusivity, Heat Capacity and Thermal Conductivity, *J.Appl. Physics*, vol. 32, 1961, pp. 1679-1684.

[11] B.M. Suleiman, S. Malinarić. Developments in the Data Evaluation of the EDPS Technique to Determine Thermal Properties of Solids, *WSEAS Transactions on Heat and Mass Transfer*, vol. 2, no. 4, April 2007, pp. 99-110.

[12] W.P. Winfree, J.N. Zalameda, Single Sided Thermal Diffusivity Imaging in Composites with a Shuttered Thermographic Inspection system, *Proc. SPIE «Thermosense-XXIV»*, vol. 4710, 2002, pp. 536-544.